ACS APPLIED NANO MATERIALS
Cite This: ACS Appl. Nano Mater. 2018, 1, 4435−4441
Article
www.acsanm.org

Graphene−Carbon Nanotube Aerogel with a Scroll-Interconnected-Sheet Structure as an Advanced Framework for a High-Performance Asymmetric Supercapacitor Electrode

Wei Fan,[†] Yiqin Shi,[†] Wei Gao,[‡] Zhen Sun,[†] and Tianxi Liu*[,†]

[†]State Key Laboratory for Modification of Chemical Fibers and Polymer Materials, College of Materials Science and Engineering, Innovation Center for Textile Science and Technology, Donghua University, 2999 North Renmin Road, Shanghai 201620, P. R. China

[‡]State Key Laboratory of Molecular Engineering of Polymers, Department of Macromolecular Science, Fudan University, 220 Handan Road, Shanghai 200433, P. R. China

Supporting Information

ABSTRACT: Carbon nanomaterials have received much attention due to their good electrochemical performance as electrode materials and as substrates for pseudocapacitive materials. Herein, the graphene−carbon nanotube aerogel (GCA) has been constructed by direct cryodesiccation from the aqueous dispersion of a graphene oxide−carbon nanotube hybrid, the so-called "sol-cryo" method, followed by high-temperature carbonization. The as-obtained GCA with a unique sheet-scroll conjoined architecture not only displays an excellent electrical double-layer capacitive performance but also performs as an ideal three-dimensional template for the perpendicular immobilization of $Ni(OH)_2$ nanosheets. The capacitance of $Ni(OH)_2$@GCA is 1208 F g^{-1} at 1 A g^{-1} with 88% retention after 2000 cycles. The $Ni(OH)_2$@GCA//GCA asymmetric supercapacitor exhibits a high energy density of 30 Wh kg^{-1} at a power density of 820 W kg^{-1}. In addition, this template-free sol-cryo method possesses simplicity and large-scale availability, which provides a novel approach for fabricating macroscopic electrode materials for supercapacitors.

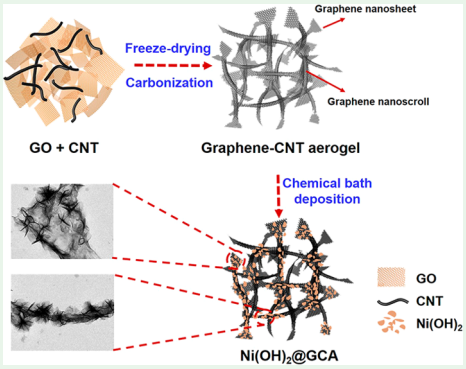

KEYWORDS: *graphene, aerogel, carbon nanotubes, sheet-scroll, asymmetric supercapacitor*

INTRODUCTION

Supercapacitors have drawn wide attention with their good power density, long lifetime, and rate capability[1−3] and can be categorized as electrical double-layer capacitors (EDLCs) and pesudocapacitors in terms of charge-storage mechanisms.[4−6] EDLCs with excellent cyclic and rate performances but poor capacitance consist of carbon materials, such as graphene, carbon nanotubes (CNTs), and carbon aerogels.[7−13] Pesudocapacitors include metal oxides, metal hydroxides, and conducting polymers such as $Ni(OH)_2$,[14−19] Co_3O_4,[20,21] and polyaniline,[22−24] which exhibit a higher charge-storage ability but poor stability. Among these materials, $Ni(OH)_2$ with a high theoretical capacity stands out as an ideal candidate for its application as a supercapacitor.[17] However, morphologies of electrode materials can greatly affect the electrochemical performance.[25,26] Pure $Ni(OH)_2$ usually forms severe aggregates that inhibit the full exposure of its electrochemically active sites. In addition, $Ni(OH)_2$ has a very small electrochemical voltage window (0−0.5 V), which will cause a low energy density and hamper its practical applications.[19] One of the strategies to solve both problems is to hybridize $Ni(OH)_2$ with carbon nanomaterials, which can tailor $Ni(OH)_2$ to a nanostructured morphology that provides a larger contacting area with the electrolyte and a shorter ion diffusion pathway, thus improving the capacitance of the electrode. Assembling the asymmetric supercapacitor (ASC) with carbon nanomaterials as the negative electrodes can provide a wider working voltage.[27,28] As a result of both the improved capacitance and the operating voltage, the energy density can be significantly increased.

With the benefit of specific area and conductivity, three-dimensional (3D) carbon frameworks (such as graphene aerogels) are promising candidates as substrates for $Ni(OH)_2$ nanosheets (noted as $Ni(OH)_2$ NSs) and suitable negative electrodes.[29] The graphene-based aerogels have been obtained by hydrothermal means, direct ink writing, chemical vapor deposition, and ascorbic reduction.[30−34] However, graphene sheets are easily restacked during the synthesis of the aerogel in many cases. Hence, CNTs are used as spacers to prevent graphene sheets from restacking in previous reports.[35−37] Additional mesopores can be obtained by adding CNTs into the aerogel, which further improves the impregnation of the

Received: April 11, 2018
Accepted: September 5, 2018
Published: September 5, 2018

DOI: 10.1021/acsanm.8b00605
ACS Appl. Nano Mater. 2018, 1, 4435−4441

electrolyte, resulting in improved electrochemical performance. Besides, CNTs could also facilitate electron transport across the whole aerogel by interconnecting adjacent graphene sheets. However, those 3D graphene−CNT hybrid structures are usually fabricated by either energy/time-consuming chemical vapor deposition, a vacuum filtration process, or a process involving surfactant modification, which hampers the overall conductivity of the obtained hybrid. Therefore, a facile and energy-saving method for constructing 3D graphene−CNT hybrids is preferred for large-scale applications.

In this work, 3D graphene−CNT aerogel (GCA) has been fabricated by a sol-cryo approach followed by high-temperature carbonization, which is further employed as a conductive framework for $Ni(OH)_2$ immobilization (schematically illustrated in Figure 1). In this process, the GCA is directly formed

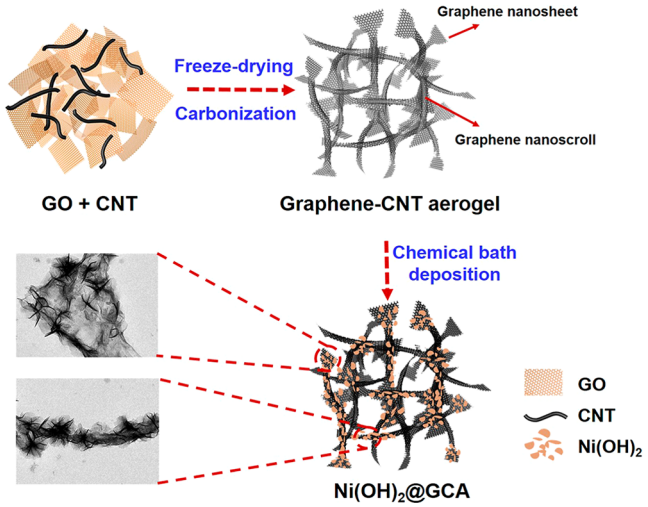

Figure 1. Schematic for the preparation of the $Ni(OH)_2$@GCA composite.

from the aqueous solution by cryodesiccation, that is, the sol-cryo method, rather than from the hydrogels generally needed in previous methods. In particular, because of the rapid freezing process, the GCA forms a 3D network with a unique graphene nanoscroll-interconnected-nanosheet structure, between which CNTs are inserted homogeneously. CNTs can further improve the conductivity of the aerogel and hinder the restacking of graphene layers, producing mesopores by intercalating between graphene nanosheets or becoming enwrapped by graphene nanoscrolls. The all-carbon framework serves as a good matrix for the immobilization of $Ni(OH)_2$, favoring the access of the electrolyte. As a result, the capacitance of $Ni(OH)_2$@GCA is up to 1208 F g^{-1} (1 A g^{-1}). Moreover, an ASC of $Ni(OH)_2$@GCA and the GCA electrode possesses a maximum energy density of 30 Wh kg^{-1}.

EXPERIMENTAL SECTION

Preparation of the Graphene−CNT Aerogel (GCA). The GCA was prepared according to our previous work (see details in the Supporting Information).[31] Briefly, CNT dispersion (4 mg mL^{-1}) and graphene oxide (GO) dispersion (8 mg mL^{-1}) were first prepared. The GO and CNT dispersions were mixed in a volume ratio of 1:1 and then put into liquid nitrogen for shock cooling, followed by freeze-drying. The GCA is obtained by heating the GO−CNT aerogel at 800 °C for 2 h. The pure graphene aerogel (CA) without CNTs was also made by following the same approach.

Synthesis of the $Ni(OH)_2$@GCA Composite. The composite was synthesized by chemical bath deposition. Briefly, 290 mg of $Ni(NO_3)_2{\cdot}6H_2O$ and 180 mg of $CO(NH_2)_2$ were dispersed in 30 mL of an ethanol/DI (deionized) water (v/v 2:1) mixture. The GCA was added to the dispersion, which was held at 70 °C for 8 h. Afterward, the as-obtained $Ni(OH)_2$@GCA-1 was collected. To obtain composites with various loadings of $Ni(OH)_2$, 580 and 1160 mg of $Ni(NO_3)_2{\cdot}6H_2O$ and 360 and 540 mg of $CO(NH_2)_2$ were applied, respectively, and the resulting samples were identified as $Ni(OH)_2$@GCA-2 and $Ni(OH)_2$@GCA-3. The $Ni(OH)_2$ sample was fabricated without adding the GCA.

Electrochemical Measurements. The tests are conducted in a 6 M KOH solution with Hg/HgO and Pt as a reference and a counter electrode, respectively. The $Ni(OH)_2$@GCA composites were cut into slices with an area of 10 mm × 10 mm and used directly as an electrode material, followed by compression on stainless steel foil with a mass loading of about 1.2 mg for a single electrode. The electrochemical performance was tested by a CHI 660D electrochemical workstation. The ASC obtained by employing $Ni(OH)_2$@GCA and GCA as the positive and negative electrode was characterized according to our previous work.[38]

RESULTS AND DISCUSSION

Morphology and Microstructure of the $Ni(OH)_2$@GCA Composite. The GCA was obtained through the quick freezing of the mixture of the GO/CNT aqueous dispersion directly, followed by lyophilization and high-temperature carbonization. In an overview, the pore size of a 3D porous GCA varies from dozens of micrometers to hundreds of nanometers (Figure 2A). Specifically, the microstructure of a GCA was conjoined by the graphene nanoscrolls and graphene nanosheets. It is believed that during the quenching process the GO sheets partially roll up into a tubular structure, and the nanosheets and nanoscrolls are conjoined together, resulting in a 3D network. During calcination, the oxygen-containing groups on CNTs were removed and GO was reduced to graphene, while the graphene nanoscroll-interconnected-nanosheet network was well retained. In contrast to the smooth graphene sheet in a GA (Figure S1A,B), the surface of the graphene sheet in a GCA is much rougher, leading to a larger surface area. As displayed in Figure S1C,D, CNTs distribute homogeneously on the graphene sheets, suggesting a good dispersibility of CNTs and graphene. TEM images also show that the uniformly dispersed CNTs are either intercalated between graphene nanosheets (Figure 2B) or enwrapped by graphene nanoscrolls (Figure 2C). In this way, CNTs can prevent the restacking of graphene layers to improve the exposed surface area and produce some mesopores. Furthermore, the CNTs intertwining and bridging with graphene could improve the conductivity of the aerogel as the conductivity increases from 56 S m^{-1} of GA to 120 S m^{-1} of GCA, thus facilitating the electron transfer.

The structure of $Ni(OH)_2$@GCA hybrids was revealed in Figure 2D−F. The inset in Figure 2D shows the digital photo of the $Ni(OH)_2$@GCA composite, indicating its good structural integrity. The $Ni(OH)_2$ sheets form well-defined, ultrathin sheet-like architectures with sizes from 400 to 500 nm by using the GCA as a substrate. The 3D porous structure of the aerogel was well retained with a proper loading of $Ni(OH)_2$ NSs, which are loaded homogeneously onto both graphene nanosheets and graphene nanoscrolls (Figure 2D−F). From the TEM images (Figure 2G−I), $Ni(OH)_2$ NSs are vertically adhered onto both graphene nanosheets and the outer wall of graphene nanoscrolls. EDX results also indicate that $Ni(OH)_2$ NSs have an even distribution on the whole

DOI: 10.1021/acsanm.8b00605
ACS Appl. Nano Mater. 2018, 1, 4435−4441

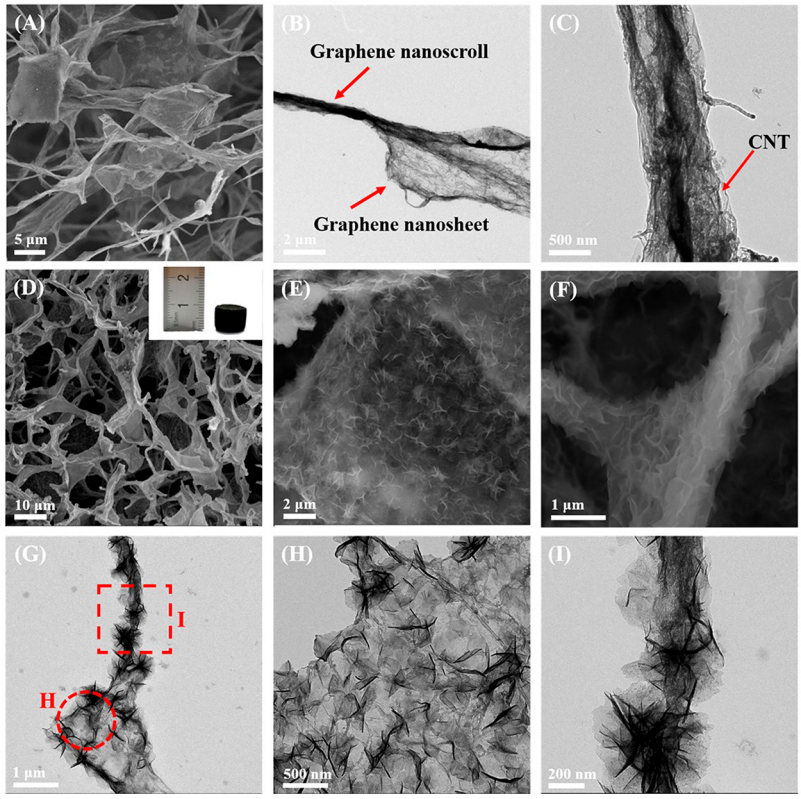

Figure 2. (A) SEM and (B, C) TEM images of GCA. SEM images of $Ni(OH)_2$@GCA-2 at (D) low and (E, F) high magnifications. The inset shows the digital photo of a freestanding $Ni(OH)_2$@GCA composite. (G–I) TEM images of $Ni(OH)_2$@GCA-2. (H, I) Enlarged view of the indicated circled and squared areas (G), indicating that $Ni(OH)_2$ can grow on both graphene nanosheets and nanoscrolls.

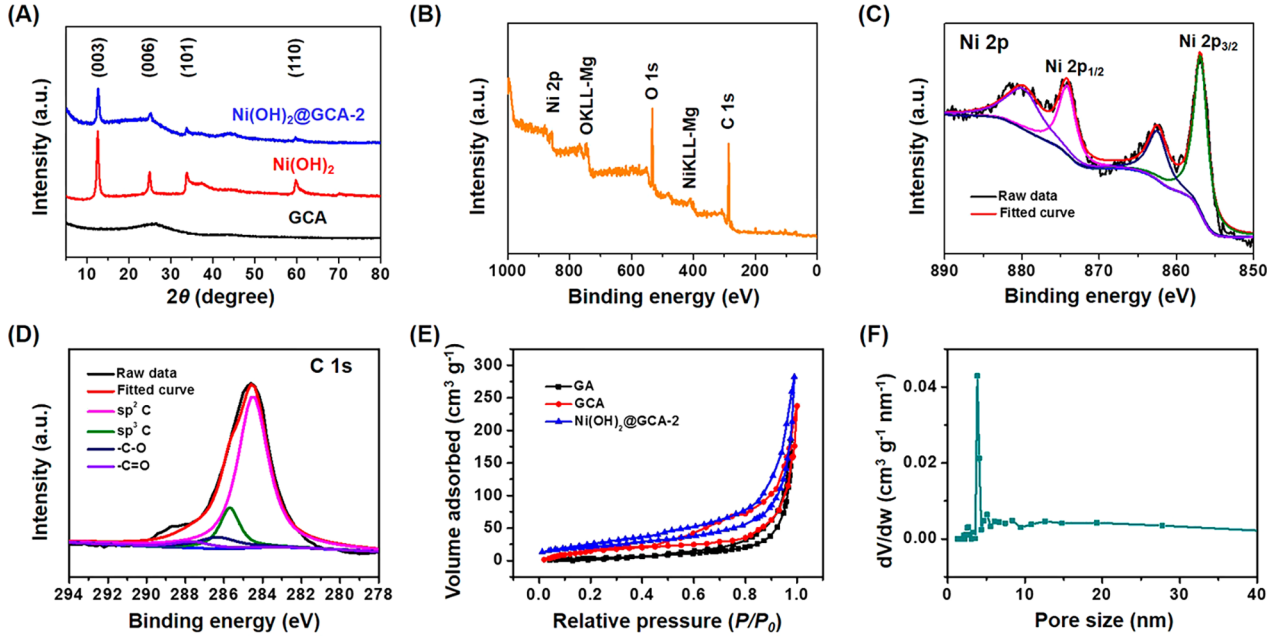

Figure 3. (A) XRD patterns of GCA, pure $Ni(OH)_2$, and $Ni(OH)_2$@GCA-2. XPS spectra of $Ni(OH)_2$@GCA-2: (B) survey scan, (C) high-resolution Ni 2p spectrum, and (D) high-resolution C 1s spectrum. (E) Nitrogen adsorption isotherms of GA, GCA, and $Ni(OH)_2$@GCA-2. (F) Corresponding pore size distribution of the $Ni(OH)_2$@GCA-2 composite.

skeleton (Figure S2). For $Ni(OH)_2$@GCA-1, few $Ni(OH)_2$ NSs are randomly loaded onto a GCA (Figure S3A,B). The sample obtained by the increased addition of Ni-based salt and urea shows that the overloading of $Ni(OH)_2$ destroys the porous structure (Figure S3C,D).

From Figure 3A, the GCA shows a broad and flat peak at $2\theta = 26.4°$ that is the (002) plane of the carbon. As for $Ni(OH)_2$@GCA-2, it has diffraction patterns similar to those of $Ni(OH)_2$, suggesting that the $Ni(OH)_2$ NSs are loaded onto the GCA. The XPS result in Figure 3B shows that C, Ni, and O

DOI: 10.1021/acsanm.8b00605
ACS Appl. Nano Mater. 2018, 1, 4435–4441

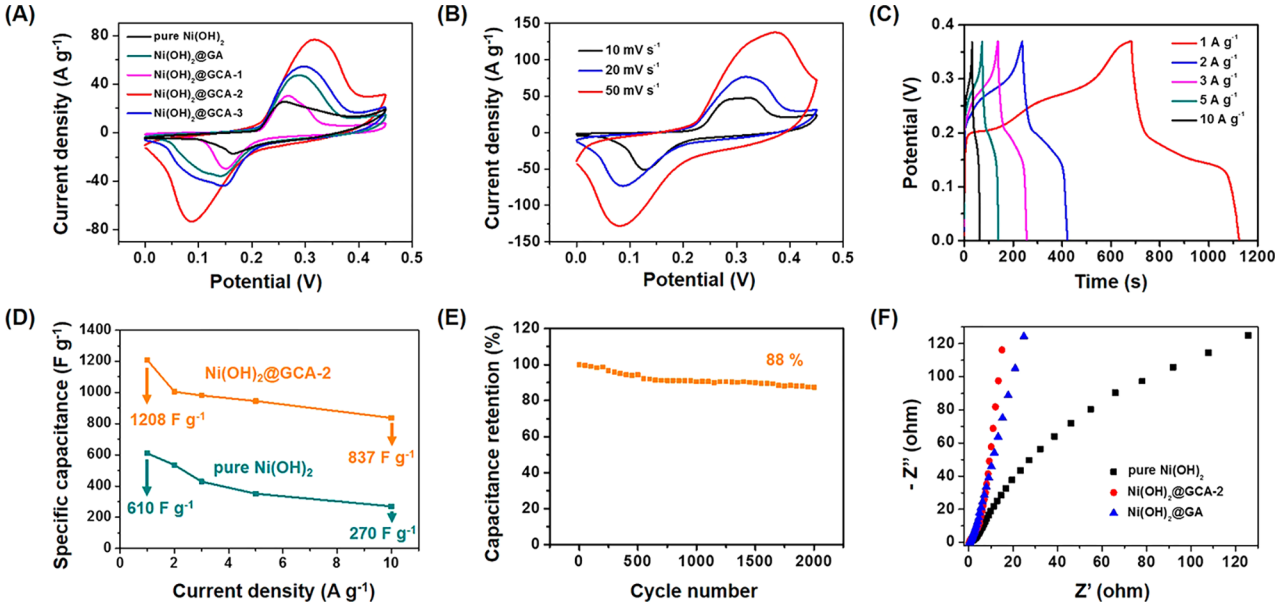

Figure 4. Electrochemical performance of the $Ni(OH)_2$@GCA-2 positive electrode. (A) CV curves of pure $Ni(OH)_2$, $Ni(OH)_2$@GA, and $Ni(OH)_2$@GCA-1,2,3 at a scan rate of 20 mV s^{-1}, (B) CV curves of $Ni(OH)_2$@GCA-2 at different scan rates from 10 to 50 mV s^{-1}, (C) galvanostatic charge−discharge curves of $Ni(OH)_2$@GCA-2 at different current densities from 1 to 10 A g^{-1}, (D) specific capacitance of pure $Ni(OH)_2$ and $Ni(OH)_2$@GCA-2 at different current densities, (E) cycling performance of $Ni(OH)_2$@GCA-2 measured at a scan rate of 200 mV s^{-1} for 2000 cycles, and (F) Nyquist plots of pure $Ni(OH)_2$, $Ni(OH)_2$@GCA-2, and $Ni(OH)_2$@GA.

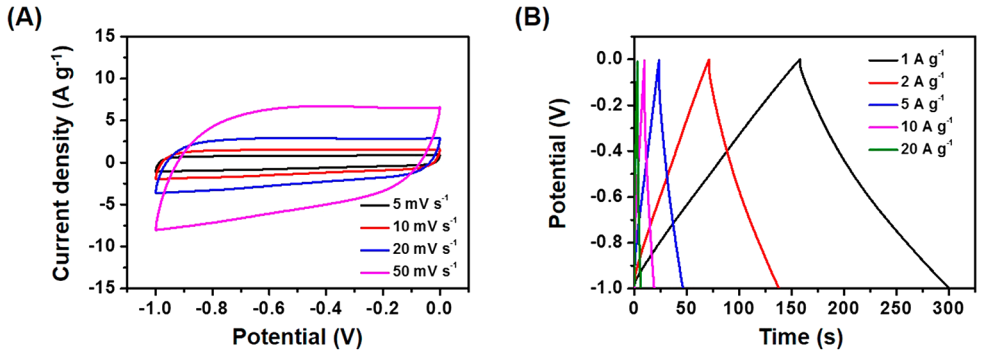

Figure 5. Electrochemical performance of the GCA negative electrode. (A) CV curves of GCA at different scan rates from 5 to 50 mV s^{-1} and (B) galvanostatic charge−discharge curves of GCA at different current densities from 1 to 20 A g^{-1}.

coexisted in the composite. The Ni 2p spectrum (Figure 3C) exhibits two peaks related to Ni $2p_{3/2}$ and Ni $2p_{1/2}$, revealing the presence of Ni^{2+}. From C 1s results (Figure 3D), the major composition of the characteristic C 1s is nonoxygenated carbon and the intensity of C−O is dramatically reduced, indicating the successful removal of the oxygen-containing groups. From Figure 3E, the surface area of the GCA (247 m^2 g^{-1}) is larger compared with that of the GA (131 m^2 g^{-1}), possibly due to the fact that CNTs intercalating between graphene can effectively prevent them from restacking. The pore size of $Ni(OH)_2$@GCA-2 is approximately 4 nm, which is in the mesoporous range (Figure 3F). This mesoporous architecture of the composite is favorable for utilization as electrode materials, which can promote ion diffusion.

Electrochemical Performance of Positive Electrode Materials. From Figure 4A, redox reaction peaks are seen in cyclic voltammetry (CV) results, suggesting that charge storage is related with the Faradaic redox reactions of $Ni(OH)_2$:

$$\alpha\text{-}Ni(OH)_2 + OH^- \leftrightarrow \gamma\text{-}NiOOH + H_2O + e^- \quad (1)$$

Among all samples, $Ni(OH)_2$@GCA-2 has the largest CV curve area, indicating the maximum capacitance, which can be due to the proper amount of $Ni(OH)_2$ on the sheet-scroll conjoined skeleton of a GCA. As for $Ni(OH)_2$@GCA-1, a lower pseudocapacitive capacitance is obtained from $Ni(OH)_2$ because of the small loading of $Ni(OH)_2$ NSs, while for $Ni(OH)_2$@GCA-3, the severe aggregation of $Ni(OH)_2$ NSs can lead to a deceased performance of electrode materials. It is observed from Figure 4B that with the increase in scan rates the CV curve shapes of $Ni(OH)_2$@GCA-2 almost do not change, demonstrating that the composites have excellent electron conduction and a small equivalent series resistance.

The galvanostatic charge−discharge test for evaluating the capacity of the $Ni(OH)_2$@GCA-2 composite is revealed in Figure 4C. The capacitance is 1208 F g^{-1} at 1 A g^{-1}. Notably, a 69% capacitance is retained at 10 A g^{-1} for the composite in comparison to 44% for bare $Ni(OH)_2$ (Figure 4D). The composite exhibits an 88% retention of its capacitance after 2000 cycles of the CV test (Figure 4E). As displayed in the Nyquist plots (Figure 4F), the composite exhibits a more vertical line than that of $Ni(OH)_2$ in a low-frequency area,

DOI: 10.1021/acsanm.8b00605
ACS Appl. Nano Mater. 2018, 1, 4435−4441

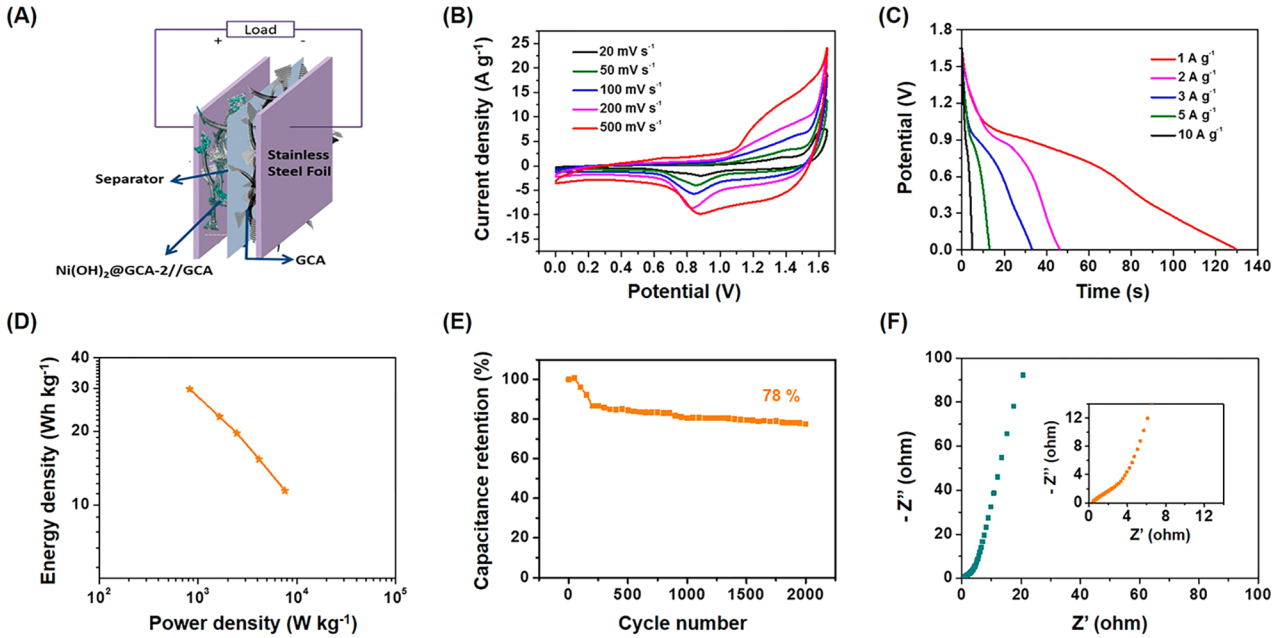

Figure 6. Electrochemical performance of the $Ni(OH)_2$@GCA-2//GCA asymmetric supercapacitor: (A) schematic of the assembled structure of an asymmetric supercapacitor based on $Ni(OH)_2$@GCA-2 as the positive electrode material and GCA as the negative material, (B) CV curves at different scan rates from 20 to 500 mV s^{-1}, (C) galvanostatic charge−discharge curves with a cell voltage of 1.6 V at current densities varying from 1 to 10 A g^{-1}, (D) Ragone plot, (E) cycling performance measured at a scan rate of 200 mV s^{-1} for 2000 cycles, and (F) Nyquist plots.

indicating better performance. Furthermore, the composite possesses an improved performance compared to that of $Ni(OH)_2$@GA, indicating an improved conductivity by adding the CNTs.

In summary, the outstanding performance of the composite is mainly owing to the following aspects. First, $Ni(OH)_2$ NSs loaded vertically onto a conductive skeleton can maximize the utilization of their high pseudocapacitance. Second, the 3D porous carbon matrix favors the diffusion of electrolyte ions and facilitates charge transfer. Finally, the unique nanosheet-interconnected-nanoscroll structure offers a high electrical conductivity pathway for facilitating the rapid charge transfer in the electrode.

Electrochemical Performance of Negative Electrode Materials. The CV curves of the GCA sample show rectangular shapes and maintain well even at high scan rates, suggesting excellent EDL capacitance behavior (Figure 5A). The capacitance of the GCA from charge−discharge curves is 149 F g^{-1}. Moreover, the absence of CNTs reflects a lower capacitance in comparison to that of the GCA (Figure S4), indicating that the existence of CNTs is favorable for the capacitance of graphene aerogels. The improved electrochemical behavior of GCA possibly results from their unique sheet-scroll conjoined architecture with a highly porous structure and good conductivity.

Electrochemical Performance of Asymmetric Supercapacitors. An ASC was assembled utilizing the $Ni(OH)_2$@GCA-2 and GCA electrodes (Figure 6A). CV curves with various voltage windows were exhibited in Figure S5 to evaluate the optimized operating voltage of the ASC. At the voltage of 1.6 V, the existence of redox peaks indicates faradic reactions coming from the positive electrode. The evolution of oxygen would occur when the voltage is above 1.8 V. Hence, an operating potential of 1.6 V of the asymmetric device is selected to further conduct the electrochemical tests.

The CV curves of the ASC show a quasi-rectangular shape, and the curve shape is well maintained at high scan rates (Figure 6B). The capacitance of the ASC is 81 F g^{-1} at 1 A g^{-1} (Figure 6C). The negative electrode (GCA) has a unique sheet-scroll conjoined architecture with a highly porous structure and good conductivity, which delivers an excellent double-layer specific capacitance. The positive electrode ($Ni(OH)_2$@GCA-2) maximizes the utilization of its high pseudocapacitance, which benefits from the highly dispersed and perpendicularly oriented $Ni(OH)_2$ NSs. Figure 6D presents Ragone plots of the ASC performed in the operating potential of 0−1.6 V. The ASC displays energy densities of 30 and 10 Wh kg^{-1} at 820 and 7590 W kg^{-1}, respectively. The performance of the device is comparable to those of previous works about $Ni(OH)_2$-related ASCs, which includes works about $Ni(OH)_2$//activated carbon (AC),[17] $Ni(OH)_2$/AC/CNT//AC,[18] and CNT/$Ni(OH)_2$//rGO[19] (Table S1). After 2000 cycles, the ASC still exhibits a high capacitive retention of 78% (Figure 6E). The Nyquist plots of the ASC were shown in Figure 6F to study the electron and ion diffusion behavior during the charge−discharge process. There are no semicircles in the high-frequency area, demonstrating a rapid charge transfer from the electrode and the electrolyte. While in a low-frequency area, the line is almost parallel to the vertical axis, indicating an excellent performance of the supercapacitor.

CONCLUSIONS

The GCA with a unique nanoscroll-interconnected-nanosheet structure has been prepared through a facile sol-cryo method, which has been utilized as a 3D porous skeleton for anchoring $Ni(OH)_2$ NSs. The as-obtained GCA with a unique sheet-scroll conjoined architecture not only provides a fast electron and ion diffusion pathways but also maximizes the exposure of the active site on $Ni(OH)_2$. With the benefit of both $Ni(OH)_2$ and the GCA, the capacitance of $Ni(OH)_2$@GCA is up to 1208 F g^{-1} at 1 A g^{-1}. The $Ni(OH)_2$@GCA//GCA ASC

DOI: 10.1021/acsanm.8b00605
ACS Appl. Nano Mater. 2018, 1, 4435−4441

shows an energy density of 30 Wh kg^{-1} at 820 W kg^{-1}. Hence, an alternative approach for fabricating macroscopic electrode materials is proposed.

■ ASSOCIATED CONTENT

Supporting Information

The Supporting Information is available free of charge on the ACS Publications website at DOI: 10.1021/acsanm.8b00605.

Experimental content; SEM images of GA, GCA, $Ni(OH)_2$@GCA-2, $Ni(OH)_2$@GCA-1, and $Ni(OH)_2$@GCA-3 samples; CV and galvanostatic charge−discharge results of GA and GCA; CV tests of the Ni(OH)@GCA-2//GCA asymmetric device; and the comparison of the electrochemical property of a previously reported asymmetric supercapacitor with $Ni(OH)_2$ electrodes (PDF)

■ AUTHOR INFORMATION

Corresponding Author

*E-mail: txliu@dhu.edu.cn; txliu@fudan.edu.cn.

ORCID

Wei Fan: 0000-0001-6978-1405

Tianxi Liu: 0000-0002-5592-7386

Notes

The authors declare no competing financial interest.

■ ACKNOWLEDGMENTS

The authors are grateful for the financial support from the National Natural Science Foundation of China (21704014, 51433001, and 21674019), the Fundamental Research Funds for the Central Universities (2232017D-06), the Shanghai Sailing Program (17YF1400200), the Program of Shanghai Academic Research Leader (17XD1400100), and the Science and Technology Commission of Shanghai Municipality (16520722100).

■ REFERENCES

(1) Ghouri, Z. K.; Barakat, N. A.; Kim, H. Y. Synthesis and Electrochemical Properties of MnO_2 and Co-Decorated Graphene as Novel Nanocomposite for Electrochemical Supercapacitors Application. *Energy & Environ. Focus* **2015**, *4*, 34−39.

(2) Zhao, Y.; Liu, J.; Hu, Y.; Cheng, H. H.; Jiang, C. G.; Jiang, L.; Cao, A. Y.; Qu, L. T. Highly Compression-Tolerant Supercapacitor Based on Polypyrrole-Mediated Graphene Foam Electrodes. *Adv. Mater.* **2013**, *25*, 591−595.

(3) Wang, H. L.; Casalongue, H. S.; Liang, Y. Y.; Dai, H. J. $Ni(OH)_2$ Nanoplates Grown on Graphene as Advanced Electrochemical Pseudocapacitor Materials. *J. Am. Chem. Soc.* **2010**, *132*, 7472−7477.

(4) Wu, X. L.; Jiang, L. L.; Long, C. L.; Wei, T.; Fan, Z. J. Dual Support System Ensuring Porous Co-Al Hydroxide Nanosheets with Ultrahigh Rate Performance and High Energy Density for Supercapacitors. *Adv. Funct. Mater.* **2015**, *25*, 1648−1655.

(5) Miller, J. R.; Simon, P. Electrochemical Capacitors for Energy Management. *Science* **2008**, *321*, 651−652.

(6) Zhang, H.; Liu, J.; Tian, Z. F.; Ye, Y. X.; Cai, Y. Y.; Liang, C. H. A General Strategy Toward Transition Metal Carbide/Carbon Core/Shell Nanospheres and Their Application for Supercapacitor Electrode. *Carbon* **2016**, *100*, 590−599.

(7) Zhang, L. L.; Zhou, R.; Zhao, X. S. Graphene-Based Materials as Supercapacitor Electrodes. *J. Mater. Chem.* **2010**, *20*, 5983−5992.

(8) Pan, H.; Li, J.; Feng, Y. Carbon Nanotubes for Supercapacitor. *Nanoscale Res. Lett.* **2010**, *5*, 654.

(9) Sheng, L. Z.; Jiang, L. L.; Wei, T.; Liu, Z.; Fan, Z. J. Spatial Charge Storage within Honeycomb-Carbon Frameworks for Ultrafast Supercapacitors with High Energy and Power Densities. *Adv. Energy Mater.* **2017**, *7*, 1700668.

(10) Zhao, J.; Li, Y. J.; Wang, G. L.; Wei, T.; Liu, Z.; Cheng, K.; Ye, K.; Zhu, K.; Cao, D. X.; Fan, Z. J. Enabling High-Volumetric-Energy-Density Supercapacitors: Designing Open, Low-Tortuosity Heteroatom-Doped Porous Carbon-Tube Bundle Electrodes. *J. Mater. Chem. A* **2017**, *5*, 23085−23093.

(11) Liu, Z.; Jiang, L. L.; Sheng, L. Z.; Zhou, Q. H.; Wei, T.; Zhang, B. S.; Fan, Z. J. Oxygen Clusters Distributed in Graphene with "Paddy Land" Structure: Ultrahigh Capacitance and Rate Performance for Supercapacitors. *Adv. Funct. Mater.* **2018**, *28*, 1705258.

(12) Zhao, B.; Chen, D. C.; Xiong, X. H.; Song, B.; Hu, R. Z.; Zhang, Q. B.; Rainwater, B. H.; Waller, G. H.; Zhen, D. X.; Ding, Y.; Chen, Y.; Qu, C.; Dang, D.; Wong, C. P.; Liu, M. L. A High-Energy, Long Cycle-Life Hybrid Supercapacitor Based on Graphene Composite Electrodes. *Energy Storage Mater.* **2017**, *7*, 32−39.

(13) Song, B.; Wu, F.; Zhu, Y. T.; Hou, Z. X.; Moon, K. S.; Wong, C. P. Effect of Polymer Binders on Graphene-Based Free-Standing Electrodes for Supercapacitors. *Electrochim. Acta* **2018**, *267*, 213−221.

(14) Yan, J.; Fan, Z. J.; Sun, W.; Ning, G. Q.; Wei, T.; Zhang, Q.; Zhang, R. F.; Zhi, L. J.; Wei, F. Advanced Asymmetric Supercapacitors Based on $Ni(OH)_2$/Graphene and Porous Graphene Electrodes with High Energy Density. *Adv. Funct. Mater.* **2012**, *22*, 2632−2641.

(15) Ji, J.; Zhang, L. L.; Ji, H. X.; Li, Y.; Zhao, X.; Bai, X.; Fan, X. B.; Zhang, F. B.; Ruoff, R. S. Nanoporous $Ni(OH)_2$ Thin Film on 3D Ultrathin-Graphite Foam for Asymmetric Supercapacitor. *ACS Nano* **2013**, *7*, 6237−6243.

(16) Tang, Z.; Tang, C. H.; Gong, H. A High Energy Density Asymmetric Supercapacitor From Nano-Architectured $Ni(OH)_2$/Carbon Nanotube Electrodes. *Adv. Funct. Mater.* **2012**, *22*, 1272−1278.

(17) Li, H. B.; Yu, M. H.; Wang, F. X.; Liu, P.; Liang, Y.; Xiao, J.; Wang, C. X.; Tong, Y. X.; Yang, G. W. Amorphous Nickel Hydroxide Nanospheres with Ultrahigh Capacitance and Energy Density as Electrochemical Pseudocapacitor Materials. *Nat. Commun.* **2013**, *4*, 1894.

(18) Sui, L. P.; Tang, S. H.; Chen, Y. D.; Dai, Z.; Huangfu, H. X.; Zhu, Z. T.; Qin, X. L.; Deng, Y. X.; Haarberg, G. M. An Asymmetric Supercapacitor with Good Electrochemical Performances Based on $Ni(OH)_2$/AC/CNT and AC. *Electrochim. Acta* **2015**, *182*, 1159−1165.

(19) Salunkhe, R. R.; Lin, J. J.; Malgras, V.; Dou, S. X.; Kim, J. H.; Yamauchi, Y. Large-Scale Synthesis of Coaxial Carbon Nanotube/$Ni(OH)_2$ Composites for Asymmetric Supercapacitor Application. *Nano Energy* **2015**, *11*, 211−218.

(20) Xia, H. X.; Tu, J. P.; Mai, Y. J.; Wang, X. L.; Gu, C. D.; Zhao, X. B. Self-Supported Hydrothermal Synthesized Hollow Co_3O_4 Nanowire Arrays with High Supercapacitor Capacitance. *J. Mater. Chem.* **2011**, *21*, 9319−9325.

(21) Meher, S. K.; Rao, G. R. Ultralayered Co_3O_4 for High-Performance Supercapacitor Applications. *J. Phys. Chem. C* **2011**, *115*, 15646−15654.

(22) Zhang, K.; Zhang, L. L.; Zhao, X. S.; Wu, J. S. Graphene/Polyaniline Nanofiber Composites as Supercapacitor Electrodes. *Chem. Mater.* **2010**, *22*, 1392−1401.

(23) Wu, Q.; Xu, Y. X.; Yao, Z. Y.; Liu, A. R.; Shi, G. Q. Supercapacitors Based on Flexible Graphene/Polyaniline Nanofiber Composite Films. *ACS Nano* **2010**, *4*, 1963−1970.

(24) Wang, H.; Wang, X.; Hao, Q.; Yang, X.; Lu, L. Graphene Oxide Doped Polyaniline for Supercapacitors. *Electrochem. Commun.* **2009**, *11*, 1158−1161.

(25) Yang, G.; Xu, C.; Li, H. Electrodeposited Nickel Hydroxide on Nickel Foam with Ultrahigh Capacitance. *Chem. Commun.* **2008**, *48*, 6537−6539.

(26) Zhang, L. S.; Ding, Q. W.; Huang, Y. P.; Gu, H. H.; Miao, Y. E.; Liu, T. X. Flexible Hybrid Membranes with $Ni(OH)_2$ Nanoplatelets Vertically Grown on Electrospun Carbon Nanofibers for High-

DOI: 10.1021/acsanm.8b00605
ACS Appl. Nano Mater. 2018, 1, 4435−4441

Performance Supercapacitors. *ACS Appl. Mater. Interfaces* **2015**, *7*, 22669−22677.
(27) Sheng, L. Z.; Jiang, L. L.; Wei, T.; Fan, Z. J. High Volumetric Energy Density Asymmetric Supercapacitors Based on Well-Balanced Graphene and Graphene-MnO_2 Electrodes with Densely Stacked Architectures. *Small* **2016**, *12*, 5217−5227.
(28) Liu, W.; Niu, H.; Yang, J.; Cheng, K.; Ye, K.; Zhu, K.; Wang, G. L.; Cao, D. X.; Yan, J. Ternary Transition Metal Sulfides Embedded in Graphene Nanosheets as Both the Anode and Cathode for High-Performance Asymmetric Supercapacitors. *Chem. Mater.* **2018**, *30*, 1055−1068.
(29) Xu, Y. X.; Huang, X. Q.; Lin, Z. Y.; Zhong, X.; Huang, Y.; Duan, X. F. One-Step Strategy to Graphene/$Ni(OH)_2$ Composite Hydrogels as Advanced Three-Dimensional Supercapacitor Electrode Materials. *Nano Res.* **2013**, *6*, 65−76.
(30) Xu, Y. X.; Lin, Z. Y.; Huang, X. Q.; Huang, Y.; Duan, X. F. Flexible Solid-State Supercapacitors Based on Three-Dimensional Graphene Hydrogel Films. *ACS Nano* **2013**, *7*, 4042−4049.
(31) Shi, Y. Q.; Gao, W.; Lu, H. Y.; Huang, Y. P.; Zuo, L. Z.; Fan, W.; Liu, T. X. Carbon-Nanotube-Incorporated Graphene Scroll-Sheet Conjoined Aerogels for Efficient Hydrogen Evolution Reaction. *ACS Sustainable Chem. Eng.* **2017**, *5*, 6994−7002.
(32) Guan, F. L.; An, F.; Yang, J.; Li, X.; Li, X. H.; Yu, Z. Z. Fiber-Reinforced Three-Dimensional Graphene Aerogels for Electrically Conductive Epoxy Composites with Enhanced Mechanical Properties. *Chin. J. Polym. Sci.* **2017**, *35*, 1381−1390.
(33) Min, B. H.; Kim, D. W.; Kim, K. H.; Choi, H. O.; Jang, S. W.; Jung, H. T. Bulk Scale Growth of CVD Graphene on Ni Nanowire Foams for A Highly Dense and Elastic 3D Conducting Electrode. *Carbon* **2014**, *80*, 446−452.
(34) Chen, L.; Wang, X. J.; Zhang, X. T.; Zhang, H. M. 3D Porous and Redox-Active Prussian Blue-in-Graphene Aerogels for Highly Efficient Electrochemical Detection of H_2O_2. *J. Mater. Chem.* **2012**, *22*, 22090−22096.
(35) Zhang, C.; Ren, L. L.; Wang, X. Y.; Liu, T. X. Graphene Oxide-Assisted Dispersion of Pristine Multiwalled Carbon Nanotubes in Aqueous Media. *J. Phys. Chem. C* **2010**, *114*, 11435−11440.
(36) Yang, S. Y.; Chang, K. H.; Tien, H. W.; Lee, Y. F.; Li, S. M.; Wang, Y. S.; Wang, J. Y.; Ma, C. C.; Hu, C. C. Design and Tailoring of A Hierarchical Graphene-Carbon Nanotube Architecture for Supercapacitors. *J. Mater. Chem.* **2011**, *21*, 2374−2380.
(37) Sun, H. Y.; Xu, Z.; Gao, C. Multifunctional, Ultra-Flyweight, Synergistically Assembled Carbon Aerogel. *Adv. Mater.* **2013**, *25*, 2554−2560.
(38) Lai, F. L.; Miao, Y. E.; Zuo, L. L.; Lu, H. Y.; Huang, Y. P.; Liu, T. X. Biomass-Derived Nitrogen-Doped Carbon Nanofiber Network: A Facile Template for Decoration of Ultrathin Nickel-Cobalt Layered Double Hydroxide Nanosheets as High-Performance Asymmetric Supercapacitor Electrode. *Small* **2016**, *12*, 3235−3244.

DOI: 10.1021/acsanm.8b00605
ACS Appl. Nano Mater. 2018, 1, 4435−4441